Synchronization Stability Analysis of PLL-based Grid-connected VSC System by Voltage Space Vectors

Huadong Sun, *Senior Member*, *IEEE*, Shuyan Wang, Shiyun Xu, *Member*, *IEEE*, Jingtian Bi, and Yiming Wang

***Abstract*—This paper focuses on synchronization stability analysis of the power system, in which power electronics are synchronized by the phase-locked loop (PLL). It provides new insight into the synchronization stability of power electronics from the voltage perspective. The synchronization stability analysis based on space vector is carried out by establishing a simplified model of the grid-connected voltage source converter (VSC) system. Without complex mathematical calculation, the existence criterion of equilibrium points and the criterion of transient instability dominated by the unstable equilibrium point (UEP) are derived, respectively. With the proposed method, synchronization stability can be determined by the voltage space vectors, which are more observable in potential engineering applications. At the end of this study, the steps of the synchronization stability determination by voltage space vectors are summarized, and the effectiveness and applicability of the proposed method are demonstrated by numerical simulations performed on the PSCAD/EMTDC platform.**

***Index Terms*—Large disturbance, phase locked loop (PLL), space vector, synchronization stability, voltage source converter (VSC).**

I. Introduction

GROWING share of power electronic-based generation, such as photovoltaics and wind turbines, radically changes the post-fault response of the power system [1]. Due to power electronics' multi-time-scale nonlinear switching control characteristics [2], their synchronization mechanism is apparently different from that of traditional synchronous generators. Under severe grid faults, power electronics might lose synchronism with the power grid [3], which may jeopardize the security and stability of the power grid.

Nowadays, synchronized with the grid by the phase-locked loop (PLL), grid-following converters are commonly used as interfaces between renewable energy sources and the power grid. The grid-connected voltage source converter (VSC) system is widely used in the research of the synchronization stability of PLL-based power electronics, which is usually modeled in the PLL dq coordinate system [4]. A simplified two-order analysis model of the grid-connected VSC system, similar to the rotor motion model of synchronous generators, is established in [5]. The current research mainly analyzes the stability of the simplified two-order system, which represents the synchronization stability of power electronics under large disturbances.

A considerable amount of literature has been dedicated to the research on the synchronization stability of PLL-based VSCs. For equilibrium point analysis, most research judges the existence of post-fault equilibrium points by the q-axis component of the point of common coupling (PCC) voltage. Accordingly, the range of active power and the current limit are derived in [6] and [7], respectively. For transient stability analysis, the equal area criterion (EAC) [8]–[10], the Lyapunov's direct method [11]–[13] and phase portrait method [14]–[16] are commonly used. EAC helps understand the mechanism of VSC's synchronization stability intuitively. A handful of studies propose the transient stability enhancement based on the EAC [8]–[10]. However, different from the traditional synchronous generator, the sign of the damping coefficient of VSC is uncertain [17], causing a very doubtful result with EAC [18]. In [11] and [12], the domain of attraction is calculated by proposed Lyapunov functions. The result of the Lyapunov's direct method is conservative. Still, the exact Lyapunov function for assessing the PLL-synchronized system's transient stability has not yet been developed. The phase portrait method can intuitively show the attraction domain of stable equilibrium points and unstable limit cycles [19]. The attraction area with various initial states is calculated by phase portrait in [14] and [15]. A synchronization stability control method using Thevenin equivalent parameter estimation and phase portrait method is proposed in [16]. Nevertheless, mechanism analysis cannot be made because that is a numerical method.

The angle difference between PLL's d-axis and the grid voltage vector studied in the synchronization stability analysis methods above is a function of time and the output angle of PLL. Consequently, obtaining from the local Phasor Measurement Units (PMUs) is not easy. Considering that voltage is easier to measure, a determination method for synchronization stability of PLL-based grid-connected VSC system is proposed in this paper. The relationship between the voltage and the angle studied in above methods is derived. Further, synchronization stability criteria for different transient

Manuscript received July 4, 2022; revised September 15, 2022; accepted October 10, 2022. Date of online publication March 3, 2023; date of current version March 28, 2024. This work was supported in part by the National Natural Science Foundation of China (U2166601, 51977197, 51907179).

H. D. Sun, S. Y. Wang, S. Y. Xu (corresponding author, email: xushiyun@epri.sgcc.com.cn), J. T. Bi and Y. M. Wang are with State Key Laboratory of Power Grid Safety and Energy Conservation, China Electric Power Research Institute, Beijing 100192, China.

DOI: 10.17775/CSEEJPES.2022.04450

stages after a fault are given by voltage space vector analysis. Only by monitoring the voltage, it can be judged whether the system loses synchronization stability.

The rest of the paper is organized as follows. A simplified model of VSC is introduced in Section II. A synchronization stability analysis method by space vector is proposed in Section III. Further, the criterion of equilibrium point existence and criterion of transient instability dominated by the unstable equilibrium point (UEP) are given. In Section IV, the steps of the determination method for synchronization stability of power electronics by voltage space vectors are summarized and the simulation verifications are performed. Finally, discussion and conclusion are drawn in Section V.

II. System Modeling

Figure 1 shows the structure of the grid-connected VSC system. $U_{\rm g}$, $U_{\rm PCC}$, $U_{\rm c}$, and I are vectors of equivalent grid voltage, voltage at the point of common coupling (PCC), AC side voltage, and output current of the VSC, respectively. $R_{\rm c}$, $L_{\rm c}$, and $Z_{\rm c}$ are resistance, inductance, and impedance from the VSC outlet to the PCC, respectively. $R_{\rm g}$, $L_{\rm g}$, and $Z_{\rm g}$ are resistance, inductance, and impedance from the PCC to the equivalent grid.

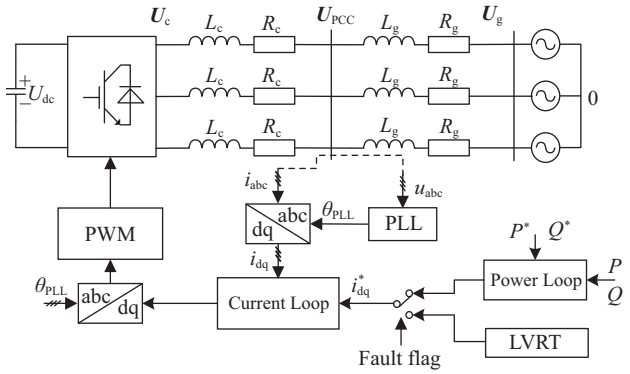

Fig. 1. Structure of grid-connected VSC system.

From now on, the subscript dq represents the components in the PLL dq coordinate system. The subscript abc represents components in the three-phase stationary coordinate frame. The subscripts 0 and 0+ represent electrical quantities before fault and at the moment fault occurs respectively. The superscript * represents reference values.

The controllers of the VSC mainly include power outer loop controller, current inner loop controller, PLL, etc. PLL samples the voltage at PCC. Suppose that the DC voltage of VSC is constant [9]. When the voltage drops as severe grid faults, the power outer loop controller is bypassed, and the current reference value of inner loop controller is given by the low voltage ride through (LVRT) control strategy instead [7]. Hence $i_{\rm d}^*$ and $i_{\rm q}^*$ can be regarded as constants during severe grid faults. Due to the fast response of the current inner loop controller, $i_{\rm d} = i_{\rm d}^*$ and $i_{\rm q} = i_{\rm q}^*$ stand in study of the PLL dynamics during grid faults [9].

The control diagram of the PLL is illustrated in Fig. 2. It is stipulated that the $\boldsymbol{U}_{\rm PCC}$ is oriented on the d-axis in the PLL dq coordinate system, and the q-axis is 90° ahead of the d-axis.

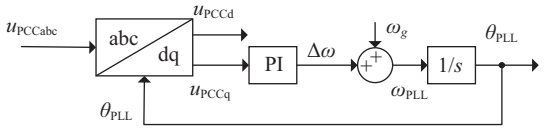

Fig. 2. Control diagram of SRF-PLL.

According to the control diagram of the PLL in Fig. 2, the second-order equation of SRF-PLL can be expressed as:

$$\begin{cases} \dfrac{{\rm d}\theta_{\rm PLL}}{{\rm d}t} = \omega_{\rm PLL} \\ \dfrac{{\rm d}\omega_{\rm PLL}}{{\rm d}t} = k_{\rm i} u_{\rm PCCq} + k_{\rm p} \dfrac{{\rm d}u_{\rm PCCq}}{{\rm d}t} \end{cases} \tag{1}$$

where $\theta_{\rm PLL}$ is the angle between d-axis of PLL dq coordinate system and negative β-axis of two-phase stationary coordinate frame, and $\omega_{\rm PLL}$ is the angle frequency of d-axis of PLL dq coordinate system. $k_{\rm i}$ and $k_{\rm p}$ are proportional and integral coefficients of PI controller of PLL respectively.

The angles mentioned in this paper is shown in Fig. 3. $\theta_{\rm g}$ is the angle between xy coordinate frame and negative β-axis of two-phase coordinate reference frame, and $\omega_{\rm g}$ is the angle frequency of xy coordinate frame.

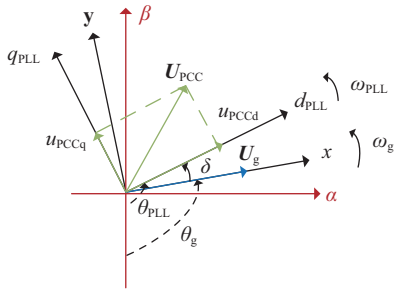

Fig. 3. Diagram of angles.

Substituting $\Delta\omega = \omega_{\rm PLL} - \omega_{\rm g}$ and $\delta = \theta_{\rm PLL} - \theta_{\rm g}$ into (1), the second-order equation can be further expressed as:

$$\begin{cases} \dfrac{{\rm d}\delta}{{\rm d}t} = \omega_{\rm PLL} - \omega_{\rm g} \\ \dfrac{{\rm d}\Delta\omega}{{\rm d}t} = k_{\rm i} u_{\rm PCCq} + k_{\rm p} \dfrac{{\rm d}u_{\rm PCCq}}{{\rm d}t} \end{cases} \tag{2}$$

Voltage equation of AC lines from the PCC to grid in the PLL dq coordinate system is

$$\begin{cases} L_{\rm g} \dfrac{{\rm d}i_{\rm d}}{{\rm d}t} = -R_{\rm g} i_{\rm d} + \omega_{\rm PLL} L_{\rm g} i_{\rm q} + u_{\rm PCCd} - u_{\rm gd} \\ L_{\rm g} \dfrac{{\rm d}i_{\rm q}}{{\rm d}t} = -\omega_{\rm PLL} L_{\rm g} i_{\rm d} - R_{\rm g} i_{\rm q} + u_{\rm PCCq} - u_{\rm gq} \end{cases} \tag{3}$$

Since current loop has a much higher bandwidth than that of PLL, current loop dynamic is usually ignored when it comes to analysis of PLL dynamic [10], that is $i_{\rm d} = i_{\rm d}^*$ and $i_{\rm q} = i_{\rm q}^*$. Further, $i_{\rm d}^*$ and $i_{\rm q}^*$ can be regarded as constants during severe grid faults. Therefore ${\rm d}i_{\rm d}/{\rm d}t = 0$, ${\rm d}i_{\rm q}/{\rm d}t = 0$, and the simplified expression of (3) can be obtained as

$$u_{\rm PCCd} = R_{\rm g} i_{\rm d} - \omega_{\rm PLL} L_{\rm g} i_{\rm q} + U_{\rm g} \cos\delta$$

$$u_{\mathrm{PCCq}} = R_{\mathrm{g}} i_{\mathrm{q}} + \omega_{\mathrm{PLL}} L_{\mathrm{g}} i_{\mathrm{d}} - U_{\mathrm{g}} \sin\delta \tag{4}$$

From (2) and (4), the second-order dynamic equation of δ for the synchronization stability analysis in this paper can be obtained as:

$$M_{\mathrm{eq}} \frac{\mathrm{d}^2\delta}{\mathrm{d}t^2} + D_{\mathrm{eq}} \frac{\mathrm{d}\delta}{\mathrm{d}t} = T_{\mathrm{eq\_a}} - T_{\mathrm{eq\_d}} \tag{5}$$

where equivalent inertia is

$$M_{\mathrm{eq}} = \frac{1 - k_{\mathrm{p}} L_{\mathrm{g}} i_{\mathrm{d}}}{k_{\mathrm{i}}} \tag{6}$$

equivalent damping is

$$D_{\mathrm{eq}} = \frac{k_{\mathrm{p}} u_{\mathrm{g}} \cos\delta}{k_{\mathrm{i}}} - L_{\mathrm{g}} i_{\mathrm{d}} \tag{7}$$

equivalent acceleration torque is

$$T_{\mathrm{eq\_a}} = \omega_{\mathrm{g}} L_{\mathrm{g}} i_{\mathrm{d}} + R i_{\mathrm{q}} \tag{8}$$

equivalent deceleration torque is

$$T_{\mathrm{eq\_d}} = U_{\mathrm{g}} \sin\delta \tag{9}$$

III. Analysis of Synchronization Stability Mechanism Based on Space Vector Relationship

As mentioned in Section I, the existing research mainly focuses on the dynamic process of δ in (5). However, the value of δ is not easy to acquire. Thus in this paper, the relationship between the synchronization stability and the voltage space vectors in the transient process is researched, and the dynamic synchronization stability criteria with the voltage space vectors are obtained.

A. Relationship of Space Vectors in Grid-Connected VSC System

Z_{g} and $\boldsymbol{I}$ can be expressed in the form of amplitudes and angles as:

$$\begin{cases} R_{\mathrm{g}} + \mathrm{j}\omega_{\mathrm{PLL}} L_{\mathrm{g}} = |Z_{\mathrm{g}}| \angle \theta_{\mathrm{Zg}} \\ i_{\mathrm{d}} + \mathrm{j} i_{\mathrm{q}} = I \angle \theta_{\mathrm{I}} \end{cases} \tag{10}$$

where $|Z_{\mathrm{g}}|$ and θ_{Zg} denote the impedance magnitude and angle from the PCC to the equivalent grid. I and θ_{I} are the magnitude and angle of the output current in the PLL dq coordinate system.

From (4), it can have

$$\begin{cases} u_{\mathrm{PCCd}} = I|Z_{\mathrm{g}}| \cos(\theta_{\mathrm{Zg}} + \theta_{\mathrm{I}}) + U_{\mathrm{g}} \cos\delta \\ u_{\mathrm{PCCq}} = I|Z_{\mathrm{g}}| \sin(\theta_{\mathrm{Zg}} + \theta_{\mathrm{I}}) - U_{\mathrm{g}} \sin\delta \end{cases} \tag{11}$$

Thus the following vector relationship can be obtained.

$$\boldsymbol{U}_{\mathrm{PCC}} = \boldsymbol{I} Z_{\mathrm{g}} + \boldsymbol{U}_{\mathrm{g}} \tag{12}$$

The output active and reactive power of VSC are

$$\begin{cases} P = \dfrac{3}{2}(u_{\mathrm{PCCd}} i_{\mathrm{d}} + u_{\mathrm{PCCq}} i_{\mathrm{q}}) \\ Q = \dfrac{3}{2}(u_{\mathrm{PCCq}} i_{\mathrm{d}} - u_{\mathrm{PCCd}} i_{\mathrm{q}}) \end{cases} \tag{13}$$

In the steady state before the fault, the active power of VSC is positive, and the reactive power is 0. According to the power equation of (13), in the PLL dq coordinate system of Fig. 3, it can be seen $i_{\mathrm{d}}^* > 0$ and $i_{\mathrm{q}}^* = 0$ obviously. So $\theta_{\mathrm{I0}} = 0$, $\theta_{\mathrm{Zg0}} + \theta_{\mathrm{I0}} > 0$. The vector relationship in the steady state before the fault is shown in Fig. 4. From the vector relationship of (12), it can be concluded that the angle δ_0 between the d axis of PLL dq coordinate system and $\boldsymbol{U}_{\mathrm{g0}}$ is positive.

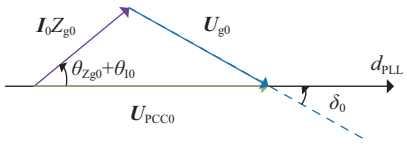

Fig. 4. The vector relationship in the steady state before the fault.

According to the output current, grid-connected impedance and grid voltage, the transient process of the grid-connected VSC system after a fault can be divided into the following three stages.

a) Stage I: during the fault.: During the fault, to supply reactive power, i_{q}^* should be negative according to (13). Usually, renewable energy sources supply few amount of active power, that is, i_{d}^* is a small positive value, and $i_{\mathrm{d}}^* \ll |i_{\mathrm{q}}^*|$. As a result, θ_{I} is negative during the fault.

Under the premise that the fault is a deep voltage drop, the following assumptions are made.

1) Within a short time after the fault occurs, ignoring the line dynamics, $|Z_{\mathrm{g}}|$ and θ_{Zg} can be regarded as constants.

2) Because i_{d}^* and i_{q}^* are determined by the LVRT control strategy during the fault and are constants, I and θ_{I} are constants.

Under the above assumptions, the space vector relationship during the fault can be obtained as Fig. 5. The amplitude and angle of $\boldsymbol{I} Z_{\mathrm{g}}$, and the amplitude of $\boldsymbol{U}_{\mathrm{g}}$, all remains unchanged. In the transient process during the fault, δ moves according to (5). The end point of the vector $\boldsymbol{U}_{\mathrm{PCC}}$, which is synthesized by $\boldsymbol{I} Z_{\mathrm{g}}$ and $\boldsymbol{U}_{\mathrm{g}}$, is located on the green dashed circle in Fig. 5. The amplitude of $\boldsymbol{U}_{\mathrm{PCC}}$ changes with δ.

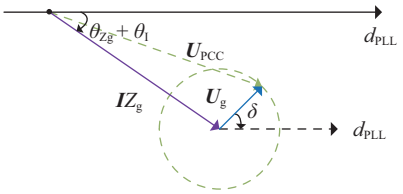

Fig. 5. The vector relationship in Stage I (during the fault).

According to Fig. 5, the amplitude of $\boldsymbol{U}_{\mathrm{PCC}}$ can be calculated as:

$$U_{\mathrm{PCC}} = \sqrt{I^2|Z_{\mathrm{g}}|^2 + U_{\mathrm{g}}^2 + 2I|Z_{\mathrm{g}}|U_{\mathrm{g}} \cos(\theta_{\mathrm{Zg}} + \theta_{\mathrm{I}} + \delta)} \tag{14}$$

It can be seen from (14) that the amplitude of $\boldsymbol{U}_{\mathrm{PCC}}$ is closely related to the value of δ. The relationship can thus be established between the voltage and the synchronization stability of the power electronics.

b) Stage II: within 20 ms after fault clearance: Due to the delay in the control switching process, the VSC will still be in LVRT strategy after the fault is cleared for about 20 ms. During this period, the grid voltage is restored to U_{g0}, and the impedance from the PCC to the equivalent grid is restored to Z_{g0}. The space vector relationship is shown in Fig. 6.

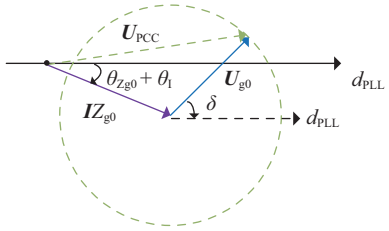

Fig. 6. The vector relationship in Stage II (within 20 ms after fault clearance).

c) Stage III: when returning to normal control: When the control strategy of VSC is switched from the LVRT strategy to the normal control after the fault, the grid-connected VSC system will return to steady state. The space vector relationship of Stage III is shown in Fig. 7.

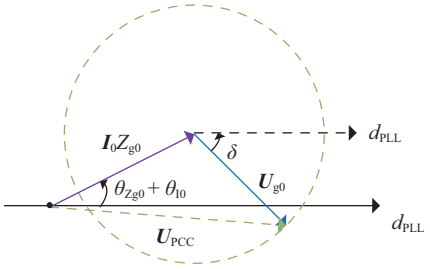

Fig. 7. The vector relationship in Stage III (when returning to normal control).

In Figs. 6 and 7, the amplitude of $\boldsymbol{U}_{PCC}$ can also be expressed in the form similar to (14). In this paper, the synchronization stability analysis in Stage I is carried out, and the conclusions obtained are also applicable in Stage II and Stage III.

B. Synchronization Stability Analysis

a) Analysis of the existence of equilibrium points: Figure 8(a), (b) and (c) are the vector relationships of the grid-connected VSC system in three different conditions in Stage I. In Fig. 8:

The purple vector is $\boldsymbol{I}Z_g$. The endpoint of the purple vector is marked as A.

The green vector is $\boldsymbol{U}_{PCC\_0+}$.

The blue vector is $\boldsymbol{U}_{g0+}$.

The red vector is $\boldsymbol{U}_{EEP}$.

The green dashed circle, whose center is A and radius is U_{g0+}, is the trajectory of endpoints of green vector $\boldsymbol{U}_{PCC\_0+}$.

The orange dashed circle, whose center is A and radius is $I|Z_g|\sin|\theta_{Zg}+\theta_I|$, is the trajectory of endpoints of red vector $\boldsymbol{U}_{EEP}$.

In Fig. 8, $\theta_{Zg}+\theta_I$ is the angle between $\boldsymbol{I}Z_g$ and d-axis of PLL dq coordinate system during the fault, and it is a negative value.

In this paper, assuming that δ does not change at the moment the fault occurs, i.e. $\delta_{0+}=\delta_0$. According to Fig. 4, the value of δ_0 in the steady state before fault can be calculated as:

$$\delta_0=\arcsin\frac{I_0|Z_{g0}|\sin(\theta_{Zg0}+\theta_{I_0})}{U_{g0}} \tag{15}$$

As shown in Fig. 5, when $\boldsymbol{U}_{PCC}$ overlaps with d_{PLL} during the fault, that is, the green dashed circle in Fig. 8 intersects with d_{PLL}, the equilibrium point of the grid-connected VSC system exists. Otherwise, the system has no equilibrium point, and the transient instability occurs.

Therefore, it can be judged that the condition shown in Fig. 8(a) has one equilibrium point, the condition shown in Fig. 8(b) has two equilibrium points, and the condition shown in Fig. 8(c) has no equilibrium point.

It can be seen from Fig. 8 that the radius of the green circle is always greater than or equal to the orange circle radius when the system has equilibrium points during the fault. Since the endpoints of $\boldsymbol{U}_{PCC\_0+}$ and $\boldsymbol{U}_{EEP}$ are on two circles, the existence of equilibrium points can also be judged by the length of these two vectors:

When $U_{PCC\_0+}=U_{EEP}$, the system has one equilibrium point.

When $U_{PCC\_0+}>U_{EEP}$, the system has two equilibrium points.

When $U_{PCC\_0+}<U_{EEP}$, the system has no equilibrium point.

Since U_{PCC_0+} changes with U_{g0+}, and U_{EEP} has nothing to do with U_{g0+}, U_{EEP} can be used as the critical value reflecting the existence of equilibrium point.

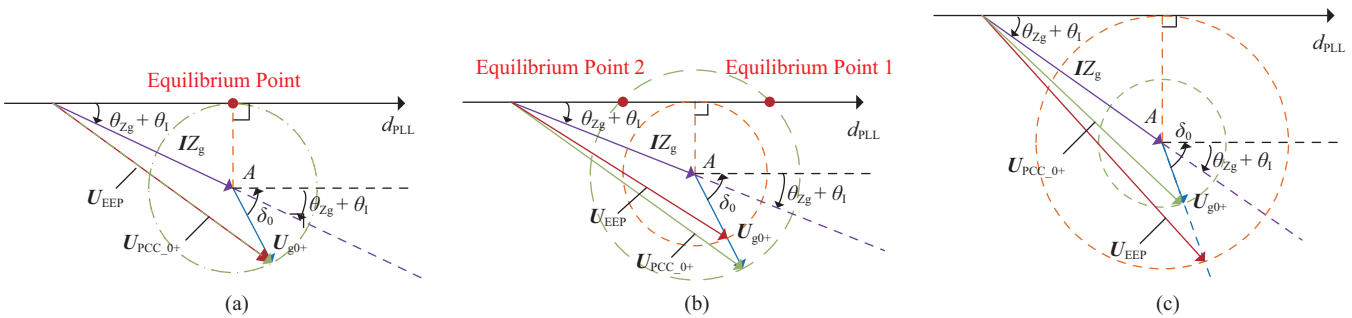

Fig. 8. The vector relationship of the grid-connected VSC system in different conditions. (a) The system with only one equilibrium point. (b) The system with two equilibrium points. (c) The system with no equilibrium point.

In Fig. 8, the length of the red vector $\boldsymbol{U}_{\mathrm{EEP}}$ can be calculated as:

$$U_{\mathrm{EEP}} = I|Z_{\mathrm{g}}|\sqrt{m} \tag{16}$$

where

$$m = 1 + \sin^2(\theta_{\mathrm{Zg}} + \theta_{\mathrm{I}}) + 2\sin|\theta_{\mathrm{Zg}} + \theta_{\mathrm{I}}|\cos(\theta_{\mathrm{Zg}} + \theta_{\mathrm{I}} + \delta_0) \tag{17}$$

If $\delta = \delta_0$, the length of the green vector $\boldsymbol{U}_{\mathrm{PCC\_0+}}$ can be calculated as:

$$U_{\mathrm{PCC\_0+}} = \sqrt{n} \tag{18}$$

where

$$n = I^2|Z_{\mathrm{g}}|^2 + U_{\mathrm{g0+}}^2 + 2I|Z_{\mathrm{g}}|U_{\mathrm{g0+}}\cos(\theta_{\mathrm{Zg}} + \theta_{\mathrm{I}} + \delta_0) \tag{19}$$

Accordingly, $U_{\mathrm{PCC\_0+}}$ can be used to determine whether there is an equilibrium point in the system during the fault. Existence criterion of two equilibrium points in the system is

$$U_{\mathrm{PCC\_0+}} > U_{\mathrm{EEP}} \tag{20}$$

When the system does not have an equilibrium point and there is only one equilibrium point, it can no longer be synchronized.

b) Small signal stability analysis for equilibrium points: If the solution starting near the equilibrium point is always maintained near it, then the equilibrium point is the stable equilibrium point (SEP), which meets the requirements of small signal stability. Otherwise, the equilibrium point is unstable equilibrium point (UEP) [20]. The stability of equilibrium points can be analyzed by the linearized system [21].

Through (2) and (4), the linearized state equation of the grid-connected VSC system is

$$\begin{bmatrix} \frac{\mathrm{d}\Delta\delta}{\mathrm{d}t} \\ \frac{\mathrm{d}\Delta\omega}{\mathrm{d}t} \end{bmatrix} = \begin{bmatrix} 0 & 1 \\ -\frac{k_{\mathrm{i}}U_{\mathrm{g}}\cos\delta_{\mathrm{e}}}{1-k_{\mathrm{p}}L_{\mathrm{g}}i_{\mathrm{d}}} & -\frac{k_{\mathrm{p}}U_{\mathrm{g}}\cos\delta_{\mathrm{e}}-k_{\mathrm{i}}L_{\mathrm{g}}i_{\mathrm{d}}}{1-k_{\mathrm{p}}L_{\mathrm{g}}i_{\mathrm{d}}} \end{bmatrix} \begin{bmatrix} \Delta\delta \\ \Delta\omega \end{bmatrix} \tag{21}$$

If and only if the real parts of all eigenvalues are negative, the equilibrium point is stable. Thus the criterion of stable equilibrium point is

$$\begin{cases} \cos\delta_{\mathrm{e}} > 0 \\ \cos\delta_{\mathrm{e}} > k_{\mathrm{i}}L_{\mathrm{g}}i_{\mathrm{d}}/(k_{\mathrm{p}}U_{\mathrm{g}}) \approx 0 \end{cases} \tag{22}$$

Namely,

$$\cos\delta_{\mathrm{e}} > 0 \tag{23}$$

Thus, if $\delta_{\mathrm{e}} \in (2k\pi - \pi/2, 2k\pi + \pi/2)$, $k \in Z$, the equilibrium point is SEP. If δ_{e} is out of that range, the equilibrium point is UEP.

c) Criterion of transient instability dominated by the unstable equilibrium point: This paper mainly studies the instability dominated by the UEP, and takes δ exceeding the UEP as the transient instability criterion. In the transient process, if δ has not surpassed UEP and operates at SEP finally, the system can recover stability after large disturbance. Once δ exceeds the UEP, the system is unstable after large disturbance.

Figure 9 is the vector relationship of the grid-connected VSC system with two equilibrium points. From (23), $\delta_{\mathrm{e\_1}}$ is the SEP and $\delta_{\mathrm{e\_2}}$ is the UEP. At the moment of the fault, assuming the angle between $\boldsymbol{U}_{\mathrm{g0+}}$ and the d_{PLL} axis is still δ_0 as in Fig. 4, $\boldsymbol{U}_{\mathrm{g0+}}$ locates on the right semicircle of the green dashed circle. After the voltage drop, the vector length of $\boldsymbol{U}_{\mathrm{g0+}}$ decreases. Because the VSC controller switches to the LVRT strategy during the fault, the amplitude and the angle of the purple vector $\boldsymbol{I}Z_{\mathrm{g}}$ will change. At this time, the q-axis component of the $\boldsymbol{U}_{\mathrm{PCC}}$ is not zero. Driven by the PLL controller, $\boldsymbol{U}_{\mathrm{g}}$ moves from the initial position $\boldsymbol{U}_{\mathrm{g0+}}$ to the direction of decreasing u_{PCCq}, that is, the direction indicated by the yellow arrow in Fig. 9. From the inherent characteristics of the second-order system, when δ moves to the SEP ($\delta_{\mathrm{e\_1}}$) for the first time, its angular velocity does not drop to zero, and it will continue to move toward the UEP. Loss of synchronism occurs if δ exceeds the UEP ($\delta_{\mathrm{e\_2}}$) before the angular velocity drops to zero.

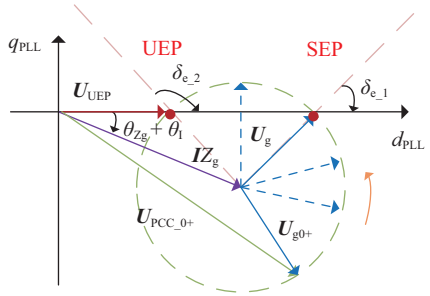

Fig. 9. Diagram of UEP and SEP during the fault.

In Fig. 9, the UEP calculated by the sine law is

$$\delta_{\mathrm{e2}} = \arcsin\frac{I|Z_{\mathrm{g}}|\sin(\theta_{\mathrm{Zg}} + \theta_{\mathrm{I}})}{U_{\mathrm{g}}} \tag{24}$$

And $\delta_{\mathrm{e\_2}} \in (2k\pi - \pi, 2k\pi - \pi/2) \cup (2k\pi + \pi/2, 2k\pi + \pi)$, $k \in Z$.

In Fig. 9, the red vector is named the reference voltage vector corresponding to the UEP, $\boldsymbol{U}_{\mathrm{UEP}}$. The length of $\boldsymbol{U}_{\mathrm{UEP}}$ can be calculated as:

$$U_{\mathrm{UEP}} = \sqrt{I^2|Z_{\mathrm{g}}|^2 + U_{\mathrm{g}}^2 + 2I|Z_{\mathrm{g}}|U_{\mathrm{g}}\cos(\theta_{\mathrm{Zg}} + \theta_{\mathrm{I}} + \delta_{\mathrm{e\_2}})} \tag{25}$$

From Fig. 9, if the length of $\boldsymbol{U}_{\mathrm{PCC}}$ is less than $\boldsymbol{U}_{\mathrm{UEP}}$, δ exceeds the UEP and the system loses synchronization stability. Thus, the transient synchronization stability can be determined with U_{PCC}. During the dynamic process, if the U_{PCC} is always satisfied as:

$$U_{\mathrm{PCC}} > U_{\mathrm{UEP}} \tag{26}$$

the system can restore synchronization stability, otherwise the system loses synchronization stability.

IV. Synchronization Stability Determination Process and Simulation Verification

A. Synchronization Stability Determination Process

The steps of synchronization stability determination of the grid-connected VSC system after a fault based on space vectors can be summarized as shown in Fig. 10.

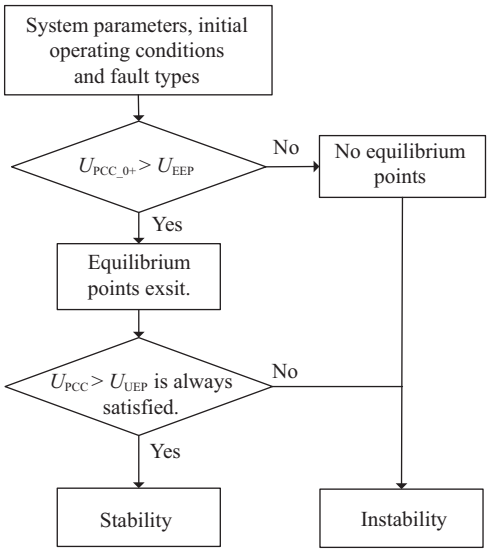

Fig. 10. Diagram of UEP and SEP during the fault.

1) Give system parameters, initial operating conditions and fault types. In practical engineering applications, system parameters during the fault can be estimated by the methods proposed in [16], [22]–[24].

2) Calculate the $U_{\mathrm{PCC\_0+}}$ and U_{EEP} at the moment when the fault occurs. If $U_{\mathrm{PCC\_0+}} < U_{\mathrm{EEP}}$, the system has no equilibrium point, and loss of synchronism will occur; if $U_{\mathrm{PCC\_0+}} > U_{\mathrm{EEP}}$, the system has an equilibrium point, and it is necessary to further judge whether δ has exceeded the UEP.

3) After the fault occurs, if the monitored voltage always satisfies $U_{\mathrm{PCC}} > U_{\mathrm{UEP}}$, the system keeps synchronously stable, otherwise synchronization instability occurs.

B. Simulation Verification

This section builds the model of the grid-connected VSC system as Fig. 1 in PSCAD/EMTDC. The parameter of the system are shown in Table I.

Set 5 cases for the simulation verification as Table II.

For case 1 to 3, the fault is not cleared, and the stability of the system is determined by Stage I. For case 4 and 5, the fault is cleared at 1.1 s. It does not matter whether Stage I and Stage II are stable or not. And the stability of the system is determined by Stage III.

For cases 1 to 5, the calculation results of the criteria for each stage are shown in Table III.

Case 1: There is no equilibrium point in Stage I.

For case 1, according to (16) and (18), $U_{\mathrm{EEP}} = 0.4483$ and $U_{\mathrm{PCC0+}} = 0.4475$ in Stage I. According to criterion (20), it can be judged that there is no equilibrium point in stage I.

TABLE I
System Parameters

Symbol	Description	Value (p.u.)
U_{g0}	Grid voltage before fault	1
U_{g}	Grid voltage during fault	0.1
R_{g0}	Resistance from the PCC to the equivalent grid before fault	0.37
L_{g0}	Inductance from the PCC to the equivalent grid before fault	0.55
R_{g}	Resistance from the PCC to the equivalent grid during fault	0.036
L_{g}	Inductance from the PCC to the equivalent grid during fault	0.12
i_{d0}	d-axis component of the output current before fault	1
i_{q0}	q-axis component of the output current before fault	0
i_{d}	d-axis component of the output current during fault	0

TABLE II
Settings

Case	i_{q} (p.u.)	Time of fault (s)	Fault clearance?	Time of fault clearance (s)	Time to switch back to normal control (s)
1	-2.8				
2	-2.5		No	–	–
3	-1	1			
4	-2.8		Yes	1.1	1.12
5	-1				

TABLE III
Calculation Results

Case	i_{q} (p.u.)	Stage	U_{EEP} (p.u.)	$U_{\mathrm{PCC0+}}$ (p.u.)	Equilibrium points exist.	U_{UEP} (p.u.)
		I	0.4483	0.4475	No	–
1 and 4	-2.8	II (for case 4)	2.7765	2.7432	No	–
		III (for case 4)	1.0719	1.4763	Yes	0.4652
2	-2.5	I	0.4003	0.4100	Yes	0.2564
		I	0.1601	0.2229	Yes	0.0267
3 and 5	-1	II (for case 5)	0.9916	1.5935	Yes	0.3790
		III (for case 5)	1.0719	1.4763	Yes	0.4652

After the fault occurs, the curves of U_{PCC} and δ are shown in Fig. 11. It can be seen that the system is unstable, which is consistent with the theoretical analysis results.

Case 2: There are equilibrium points in Stage I, but the loss of synchronism occurs.

For case 2, according to (16) and (18), $U_{\mathrm{EEP}} = 0.4003$ and $U_{\mathrm{PCC0+}} = 0.4100$ in Stage I. According to criterion (20), it can be judged that there are equilibrium points in stage I.

After the fault occurs, the curves of U_{PCC} and δ are shown in Fig. 12. It can be seen that $U_{\mathrm{PCC}} < U_{\mathrm{UEP1}}$, which does not satisfy criterion (26). The system will suffer from transient instability dominated by UEP.

Case 3: There are equilibrium points in Stage I, and the synchronism restores.

For case 3, according to (16) and (18), $U_{\mathrm{EEP}} = 0.1601$ and $U_{\mathrm{PCC0+}} = 0.2229$ in Stage I. According to criterion (20), it can be judged that there are equilibrium points in stage I of case 3.

After the fault occurs, the curves of U_{PCC} and δ are shown in Fig. 13. It can be seen that $U_{\mathrm{PCC}} > U_{\mathrm{UEP1}}$, which satisfies criterion (26). The system will not suffer from

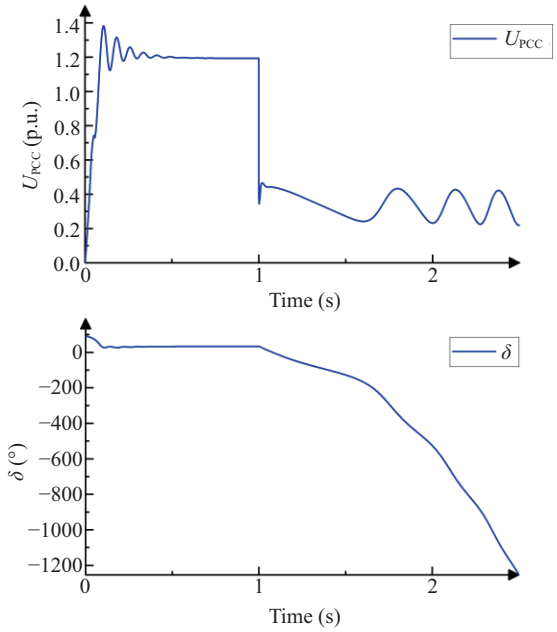

Fig. 11. Simulation results of Case 1.

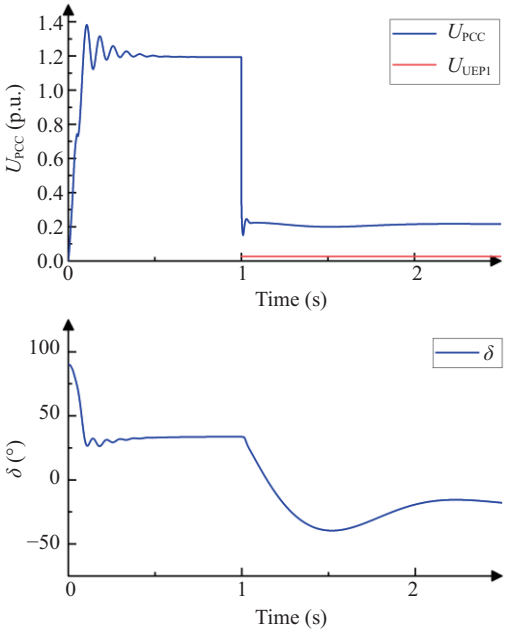

Fig. 13. Simulation results of Case 3.

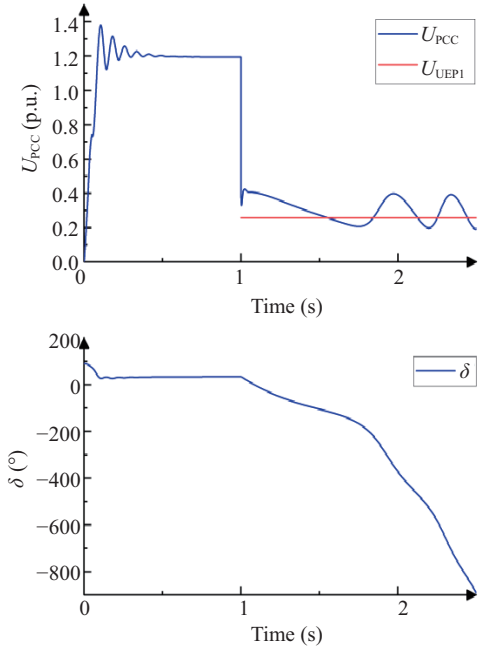

Fig. 12. Simulation results of Case 2.

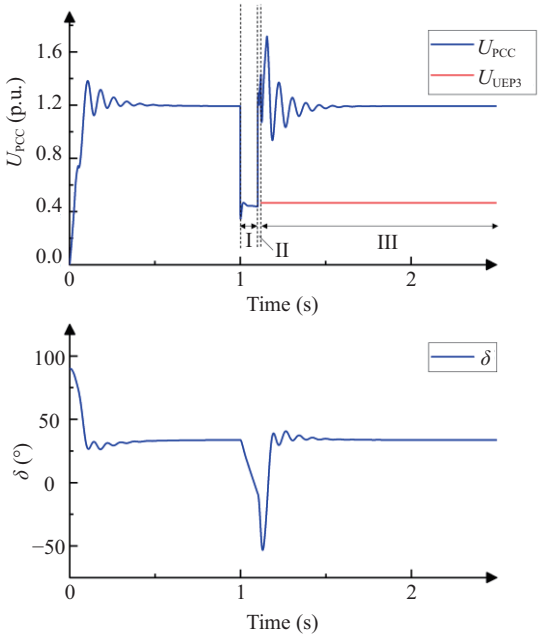

Fig. 14. Simulation results of Case 4.

transient instability dominated by UEP.

Case 4: There is no equilibrium point in Stage I Stage II. But there are equilibrium points in Stage III.

For case 4, according to (16) and (18), $U_{\mathrm{EEP}} = 1.0719$ and $U_{\mathrm{PCC0+}} = 1.4763$ in Stage III. According to criterion (20), it can be judged that there are equilibrium points in stage III. In addition, since the system parameters of Stage III are the same as that of steady state before the fault, it is easy to conclude that there are equilibrium points in Stage III without calculation.

After the fault occurs, the curves of U_{PCC} and δ are shown in Fig. 14. It can be seen that $U_{\mathrm{PCC}} > U_{\mathrm{UEP3}}$, which satisfies criterion (26). The system will not suffer from transient instability dominated by UEP. As is shown in Fig. 14, U_{UEP3} is much smaller than U_{PCC} in Stage III. Even if the system does not have any equilibrium point in Stage I and Stage II, it can eventually restore stability.

Case 5: There are equilibrium points in Stage I, II and III.

For case 5, according to (16) and (18), $U_{\mathrm{EEP}} = 1.0719$ and $U_{\mathrm{PCC0+}} = 1.4763$ in Stage III. According to criterion (20), it can be judged that there are equilibrium points in stage III. Similar to Case 4, without calculation, it can be judged that there are equilibrium points in stage III.

After the fault occurs, the curves of U_{PCC} and δ are

shown in Fig. 15. It can be seen that $U_{\mathrm{PCC}} > U_{\mathrm{UEP3}}$, which satisfies criterion (26). The system will not suffer from transient instability dominated by UEP. It can be seen from Fig. 15 that U_{UEP3} is far smaller than U_{PCC} in Stage III. Hence, it is likely to restore stability after fault clearance.

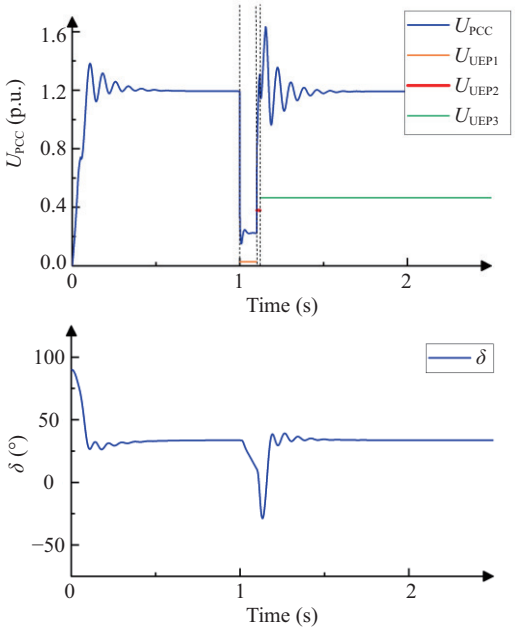

Fig. 15. Simulation results of Case 5.

Both U_{UEP} and $U_{\mathrm{PCC\_0+}}$ are related to five parameters, δ_0, I, θ_{I}, Z_{g}, and θ_{Zg}. $U_{\mathrm{PCC\_0+}}$ changes with $U_{\mathrm{g0+}}$, while U_{EEP} has nothing to do with $U_{\mathrm{g0+}}$. When the voltage drop depth and other system parameters are the same, the smaller the i_{q}, the smaller the I, the smaller the U_{EEP}, and the easier equilibrium points exist. In addition, the smaller the U_{UEP} is, the less likely it is that δ exceeds the UEP and the system loses synchronism stability.

Under the condition that the fault is not cleared, the system will experience transient instability caused by the absence of equilibrium point or dominated by the unstable equilibrium point.

V. Discussion and Conclusion

a) Discussion: At present, three types of synchronous stability determination methods for PLL-based grid-connected VSC system, including the EAC, the Lyapunov's direct method and phase portrait method, are commonly used.

For phase portrait method, the phase portrait of the second-order system relies on numerical calculation, which can clearly and intuitively display the trajectory of the system state variables, so it is not affected by whether the equivalent damping is positive or negative, but the critical clearing angle cannot be obtained by calculation. For the second-order system studied in this paper, assuming its solution is $\delta(t)$, when the system has a nontrivial periodic solution as:

$$\delta(t+T) = \delta(t),\ \forall t \geq 0 \tag{27}$$

an oscillation with period T occurs. In phase portrait, the trajectory of a periodic solution is a closed curve, usually called a periodic orbit, and an isolated periodic orbit is called a limit cycle. When t tends to infinity, all trajectories starting from any point close to the limit cycle will be far away from the limit cycle, such a limit cycle is called an unstable limit cycle. When the system has an unstable limit cycle, if the initial position of the operating point is on the limit cycle, the point will move on the limit cycle periodically; if it is outside the limit cycle, the point will move away from the limit cycle and instability after swings may occur. Therefore, the phase portrait can analyze the instability dominated by the unstable limit cycle, which is an advantage that other methods do not have.

For methods such as the EAC and the Lyapunov's direct method, the sign of the equivalent damping D_{eq} in the δ motion equation of the single VSC infinite system is related to δ, as shown in (7). And D_{eq} cannot be ignored, which is different from that of synchronous generators where D_{eq} is always positive and can be ignored. Therefore, when calculating the critical clearing angle and the critical clearing time, the EAC can only obtain a conservative boundary within the range of $D_{\mathrm{eq}} > 0$, as shown in Fig. 16. Proper selection of the Lyapunov function can expand this boundary, but it is also conservative. That type of methods is used to analyze instability dominated by UEP, but cannot analyze instability dominated by unstable limit cycles. However, its physical concept is intuitive and clear, which is of great significance for guiding and improving the PLL control to improve its synchronization stability.

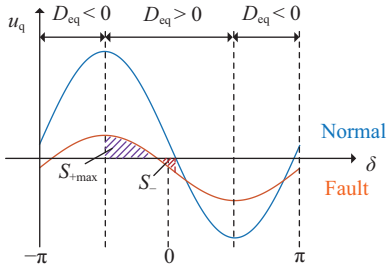

Fig. 16. Schematic diagram of the EAC.

The space vector based voltage dynamic determination method for synchronization stability proposed in this paper, by monitoring voltage at the PCC of VSC, judges whether loss of synchronism occurs in the dynamic process according to the relationship between the voltage monitored and the two reference voltages. Although the space vector method cannot realize the instability analysis dominated by unstable limit cycle and the calculation of the critical clearing angle, the method does not depend on numeral calculation and is not affected by the sign of D_{eq} in the process of dynamic discrimination. It has the following advantages:

1) The aforementioned three types of methods focus on the δ in stability analysis and calculation. The angle δ used in the above methods is a function of time and the state variable of controller, that is $\delta = \theta_{\mathrm{PLL}} - \theta_{\mathrm{g}}$. Consequently, it is not easy to obtain. However, the space vector method establishes the

TABLE IV
COMPARISON OF SEVERAL SYNCHRONOUS STABILITY ANALYSIS METHODS

Contest	EAC/Lyapunov's direct method	Phase portrait method	Space vector based method
Analysis is not affected by D_{eq}.	No.	Yes.	Yes.
Instability dominated by unstable limit cycles can be analyzed.	No.	Yes.	No.
The critical clearing angle can be calculated.	Yes, but not exactly.	No.	No.
The type of the method.	Analytical method.	Numerical method.	Dynamic discrimination.

relationship between synchronization stability and the voltage, and the required voltage information is easy to obtain.

2) Without simulation, the existence criterion of equilibrium points in the form of voltage can be used to judge whether there are equilibrium points in each stage. In the transient stability determination, only by monitoring the voltage, it can be judged whether the system loses synchronization stability. Regardless of the equivalent damping of the system, the instability occurs when the criterion of transient instability is met.

To sum up, the comparison between the voltage space vectors based method proposed in this paper and the existing synchronous stability analysis methods is shown in Table IV.

For the shortcomings of the existing synchronous stability determination methods, this paper proposes a dynamic criterion in the form of voltage, which does not require complex mathematical calculations. And this method can directly reflect the influence of synchronization stability on the external characteristics of VSC, which provides engineering insight into the analysis and determination of synchronization stability.

This study proposes a synchronization stability criterion of PLL-based grid-connected VSC system using voltage space vectors, which measuring object is easier to obtain. By determining the relationship between the voltage at PCC and the two reference voltages U_{EEP} and U_{UEP}, the synchronization stability analysis procedure of PLL-based grid-connected VSC system under large disturbance is formed, including the existence criterion of equilibrium points and the criterion of transient instability dominated by the UEP.

The reference voltage U_{EEP} and U_{UEP} are related to the pre-fault system parameters, the output current of VSC and the grid-connected impedance, and U_{UEP} is also related to the grid voltage. The electromagnetic transient simulation results show that when other parameters are the same, the larger the output current of the renewable energy source, the easier the system will lose equilibrium point. The smaller the output current of the renewable energy source, the smaller the U_{UEP}, and the less likely it is that δ exceeds the UEP and the system loses synchronism stability.

Under the condition that the fault is not cleared, the system will experience transient instability caused by the absence of equilibrium point or dominated by the unstable equilibrium point.

REFERENCES

[1] D. Pan, X. Wang, F. Liu, and R. Shi, "Transient stability of voltage-source converters with grid-forming control: A design-oriented study," *IEEE J. Emerg. Select. Top. Power Electron*., vol. 8, no. 2, pp. 1019–1033, Jun. 2020.

[2] M. Firouzi and G. B. Gharehpetian, "LVRT Performance Enhancement of DFIG-Based Wind Farms by Capacitive Bridge-Type Fault Current Limiter," *IEEE Trans. Sustain. Energy*, vol. 9, no. 3, pp. 1118–1125, Jul. 2018.

[3] D. Dong, B. Wen, D. Boroyevich, P. Mattavelli, and Y. Xue, "Analysis of phase-locked loop low-frequency stability in three-phase grid-connected power converters considering impedance interactions," *IEEE Trans. Ind. Electron*., vol. 62, pp. 310–321, Jan. 2015.

[4] J. Zhao, M. Huang, H. Yan, C. K. Tse and X. Zha, "Nonlinear and Transient Stability Analysis of Phase-Locked Loops in Grid-Connected Converters," *IEEE Trans. Power Electron*., vol. 36, no. 1, pp. 1018–1029, Jan. 2021.

[5] Q. Hu, L. Fu, F. Ma and F. Ji, "Large Signal Synchronizing Instability of PLL-Based VSC Connected to Weak AC Grid," *IEEE Trans. Power Syst*., vol. 34, no. 4, pp. 3220–3229, Jul. 2019.

[6] X. He, H. Geng, R. Li and B. C. Pal, "Transient Stability Analysis and Enhancement of Renewable Energy Conversion System During LVRT," *IEEE Trans. Sustain. Energy*, vol. 11, no. 3, pp. 1612–1623, Jul. 2020.

[7] Ö. Göksu, R. Teodorescu, C. L. Bak, F. Iov and P. C. Kjær, "Instability of Wind Turbine Converters During Current Injection to Low Voltage Grid Faults and PLL Frequency Based Stability Solution," *IEEE Trans. Power Syst*., vol. 29, no. 4, pp. 1683–1691, Jul. 2014.

[8] X. He, H. Geng, J. Xi and J. M. Guerrero, "Resynchronization Analysis and Improvement of Grid-Connected VSCs During Grid Faults," *IEEE J. Emerg. Sel. Top. Power Electron*., vol. 9, no. 1, pp. 438–450, Feb. 2021.

[9] S. Huang, J. Yao, J. Pei, S. Chen, Y. Luo and Z. Chen, "Transient Synchronization Stability Improvement Control Strategy for Grid-Connected VSC Under Symmetrical Grid Fault," *IEEE Trans. Power Electron*., vol. 37, no. 5, pp. 4957–4961, May 2022.

[10] S. Ma, H. Geng, L. Liu, G. Yang and B. C. Pal, "Grid-Synchronization Stability Improvement of Large Scale Wind Farm During Severe Grid Fault," *IEEE Trans. Power Syst*., vol. 33, no. 1, pp. 216–226, Jan. 2018.

[11] M. Z. Mansour, S. P. Me, S. Hadavi, B. Badrzadeh, A. Karimi and B. Bahrani, "Nonlinear Transient Stability Analysis of Phased-Locked Loop-Based Grid-Following Voltage-Source Converters Using Lyapunov's Direct Method," *IEEE J. Emerg. Select. Top. Power Electron*., vol. 10, no. 3, pp. 2699–2709, Jun. 2022.

[12] Y. Zhang, C. Zhang and X. Cai, "Large-Signal Grid-Synchronization Stability Analysis of PLL-Based VSCs Using Lyapunov's Direct Method," *IEEE Trans. Power Syst*., vol. 37, no. 1, pp. 788–791, Jan. 2022.

[13] B. Fan and X. Wang, "A Lyapunov-Based Nonlinear Power Control Algorithm for Grid-Connected VSCs," *IEEE Trans. Ind. Electron*., vol. 69, no. 3, pp. 2916–2926, Mar. 2022.

[14] C. Wu, X. Xiong, M. G. Taul and F. Blaabjerg, "Enhancing Transient Stability of PLL-Synchronized Converters by Introducing Voltage Normalization Control," *IEEE J. Emerg. Select. Top. Power Electron*., vol. 11, no. 1, pp. 69–78, Mar. 2021.

[15] H. Wu and X. Wang, "Design-Oriented Transient Stability Analysis of PLL-Synchronized Voltage-Source Converters," *IEEE Trans. Power Electron*., vol. 35, no. 4, pp. 3573–3589, Apr. 2020.

[16] L. Peng, Y. Li, L. Mili, Y. Tang, Y. Xu, B. Zhao and J. Li, "A Real-Time Enhanced Thevenin Equivalent Parameter Estimation Method for PLL Synchronization Stability Control in VSC," *IEEE Trans. Power Deliv.*., vol. 37, no. 4, pp. 2650–2660, Aug. 2022.

[17] Y. Liu, J. Yao, J. Pei, Y. Zhao, P. Sun, D. Zeng, S. Chen, "Transient Stability Enhancement Control Strategy Based on Improved PLL for Grid Connected VSC during Severe Grid Fault," *IEEE Trans. Energy Convers*., vol. 36, no. 1, pp. 218–229, Mar. 2021.

[18] M. G. Taul, X. Wang, P. Davari and F. Blaabjerg, "An Overview of Assessment Methods for Synchronization Stability of Grid-Connected Converters Under Severe Symmetrical Grid Faults," *IEEE Trans. Power Electron*., vol. 34, no. 10, pp. 9655–9670, Oct. 2019.

[19] M. Watanabe, Y. Mitani and K. Tsuji, "A numerical method to evaluate

power system global stability determined by limit cycle," *IEEE Trans. Power Syst*., vol. 19, no. 4, pp. 1925–1934, Nov. 2004.
[20] H. Chiang and T. Wang, "On the Number and Types of Unstable Equilibria in Nonlinear Dynamical Systems With Uniformly-Bounded Stability Regions," *IEEE Trans. on Autom. Control*, vol. 61, no. 2, pp. 485–490, Feb. 2016.
[21] E. Noldus and M. Loccufier, "A comment on the method of the closest unstable equilibrium point in nonlinear stability analysis," *IEEE Trans. on Autom. Control*, vol. 40, no. 3, pp. 497–500, Mar. 1995.
[22] D. Babazadeh, A. Muthukrishnan, P. Mitra, T. Larsson, and L. Nordström, "Real-time estimation of AC-grid short circuit capacity for HVDC control application," *IET Gener. Transmiss. Distrib*., vol. 11, no. 4, pp. 838–846, 2017.
[23] N. Hoffmann and F. W. Fuchs, "Online grid impedance estimation for the control of grid connected converters in inductive-resistive distributed power-networks using extended kalman-filter," in *Proc. IEEE Energy Convers. Congr. Expo*., 2012, pp. 922–929.
[24] L. Peng, J. Zhao, Y. Tang, L. Mili, Z. Gu, and Z. Zheng, "Real-time LCCHVDC maximum emergency power capacity estimation based on local PMUs," *IEEE Trans. Power Syst*., vol. 36, no. 2, pp. 1049–1058, Mar. 2021.

Huadong Sun received the B.Eng. and M.Eng. degrees in Electrical Engineering from Shandong University, Jinan, China, in 1999 and 2002, respectively, and the Ph.D. degree in Electrical Engineering from China Electric Power Research Institute (CEPRI), Beijing, China, in 2005. He is currently a Professor of Electrical Engineering with CEPRI. His research interests include power system analysis and control, and large-scale renewable power generation and integration.

Shuyan Wang received the B.Eng. degree from the North China Electric Power University, Beijing, China, in 2019. She is currently working toward the Ph.D. degree with CEPRI, Beijing. Her research focuses on stability and safety analysis of the power electronic-based power systems.

Shiyun Xu received the Ph.D. degree in Mechanical Systems and Control from Peking University, Beijing, China, in 2010, under the direction of Prof. Lin Huang. She was a Postdoctoral Fellow with the China Electric Power Research Institute, Beijing, China, till 2012. From 2007 to 2008, she was a Visiting Scholar with Polytechnic Institute, New York University, New York, NY, USA, hosted by Prof. Zhongping Jiang. She is currently a Senior Engineer with CEPRI, Beijing, China. Her research interests include power systems dynamic stability analysis and control with high penetration of renewable energies.

Jingtian Bi received the B.S. degree from Shandong University, Jinan, China, in 2011 and the Ph.D. degree from North China Electric Power University, Beijing, China, in 2018. He worked as a postdoctoral fellow with CEPRI, Beijing, China, till 2020. He is currently a Senior Engineer in the Power System Department, CEPRI. His interests mainly include dynamic stability analysis and control for power system with high proportion of power electronics devices.

Yiming Wang received the B.Eng. degree from the Shanghai University of Electric Power, Shanghai, China, in 2017 and the M.Eng. degree from the North China Electric Power University, Beijing, China, in 2020. He is currently working toward the Ph.D. degree with the Department of Electrical Engineering, Tsinghua University, Beijing, China. His current research interests include stability analysis of the power electronic-based power systems.